Theoretical Study of Diffusion and Adsorption Inside Nano- and Mesoporous Active Particles

Oleksiy V. Klymenko

***Abstract*—Mass transport of a target species towards and within spherical mesoporous organosilica particles and its adsorption by active sites at pore walls is investigated through the numerical solution of the pertinent mathematical model. The presented theoretical results allow the optimization of mesoporous materials to increase their capacity towards target ions or molecules and their time-efficiency.**

***Index Terms*— nanopore, adsorption, desorption, numerical simulation**

I. Introduction

THE synthesis of micro- or even nanometric structures equipped with chemically active functional sites has gained significant attention in the recent years due to unique abilities of such materials to perform selective reactions on dilute species while having appropriate active chemical ligands bound to a rigid inorganic skeleton [1]-[8]. In particular, a comparatively easy sol-gel way of preparing such materials results in spherical microparticles consisting of bundles of nano- or mesopores opening through the particle surface and lined with specifically chosen active ligands to achieve selective trapping of target ions or molecules inside the particles. Due to the large surface area of the pore walls relative to their volume such particles are able to selectively accumulate extremely high concentrations of target species even of it is present in minute quantity in the solution containing the particles [4]-[5]. This property of the mesoporous particles is of high interest for selective filtration of liquids in various applications ranging from everyday to industrial and environmental purposes.

Despite a large number of works in this area most of them rely on empirical results and classical approaches although diffusion-reaction patterns developing inside nano- and mesoporous materials as well as transport conditions at the entrances to individual nanopores significantly influence the time efficiency of such materials. Therefore considering only limiting thermodynamic capacity of nanoporous particles is not sufficient for the construction of highly efficient and selective materials for specific applications.

Manuscript received March 27, 2008.

O.V. Klymenko is with the Mathematical and Computer Modelling Laboratory, Kharkov National University of Radioelectronics, 14 Lenin Ave., Kharkov, 61166, Ukraine (phone: +38 057 702 09 69; fax: +38 057 702 10 13; e-mail: klymenko@kture.kharkov.ua).

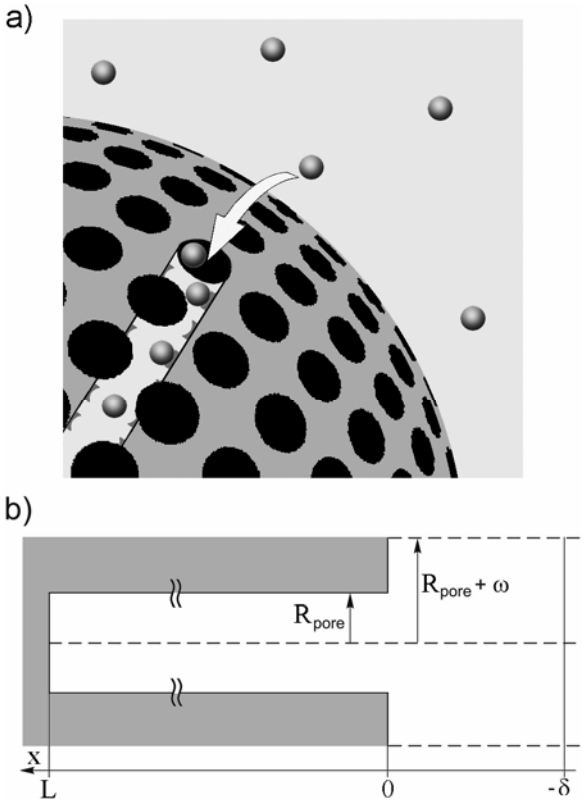

Fig. 1. Schematic representation of a spherical mesoporous particle consisting of a dense bundle of nanopores; R_{part} is the particle radius, R_{pore} that of the nanopores, L the nanopore length, ω the half-thickness of sol-gel wall and δ the thickness of the steady state diffusion layer surrounding it into the solution. (a) Schematic view showing one nanopore placement inside the particle and target species entering it from the surrounding solution. (b) Axial cross section of one nanopore and "its" diffusion layer; note that the origin of the abscissa axis, x, is fixed onto the particle surface and it is directed inside the particle; ordinates are measured orthogonally from the nanopore axis.

The general laws governing the diffusion-reaction patterns created inside such nano- or mesoporous materials during their filling and which control their cross-communications with the bulk solution (see Fig. 1) have been presented and discussed in a recent paper [9]. This general physicomathematical treatment has delineated the complex situations which may arise and outlined the general kinetic laws obeyed under each kinetic range. Its main results are presented in Fig. 2 in the form of a zone diagram depending on the two main dimensionless parameters which govern primarily the complex kinetics of diffusion and reaction within nano- or mesopores [9]. However, despite its conceptual utility the application of this general to a particular

experimental situation requires the consideration of many other parameters which affect the overall kinetic phenomena. This prevents the derivation of handy workable general laws, but nevertheless the complete model may be solved numerically. In this work we present a full numerical approach for the physicochemical problem at hand.

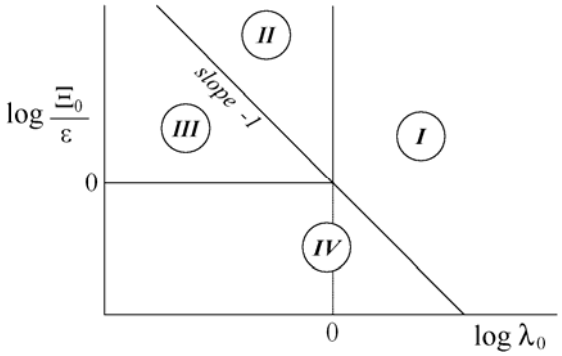

Fig. 2. (a) Kinetic zone diagram illustrating the different behaviors experienced by the 2D-nanoporous system as a function of its main dimensionless parameters characterizing its dynamics: $\Xi_0 = (2\pi R_{pore} L)\Gamma_{site} \big/ [(\pi R_{pore}^2 L) C_0^b]$ is the ratio of the quantity of species storable by the nanopore wall sites (Γ_{site} is the surface concentration of active sites) and that stored by the solution inside the nanopore at initial solution concentration C_0^b; $\varepsilon = (L/R_{pore})^2$ is the squared ratio nanopore length and its radius; and $\lambda_0 = k_{ads} L^2 C_0^b / D_{bulk}$ is the dimensionless adsorption rate constant (adapted from [9]; see below for definitions of parameters).

In practice kinetic information regarding processes occurring inside the nano- or mesoporous particles is hidden from direct observation. Thus one can access kinetic data only through measurements of the concentration of a target species in the solution bulk during a transient experiment involving vigorous solution stirring which ensures that the bulk concentration may be regarded as time-dependent only. These experimental data may be represented in the form of the quantity ratio of already extracted species and the maximum extraction capacity, $f(t) = \dfrac{Q^{tot}(\tau)}{Q_\infty^{tot}} = \dfrac{1 - c(t)}{1 - c_\infty}$, where $c(t)$ is the normalized concentration of target species at time t and c_∞ is the normalized limiting bulk concentration of target species at infinite time when complete partition equilibrium is achieved.

Since experimentally one has information only about the behavior of f we focus our analysis on this quantity and investigate its behavior as a function of dimensionless time $\tau = D_{bulk} t / L^2$ (which is related to the real time t via the target species diffusion coefficient in the bulk solution D_{bulk} and the average nanopore length $L = R_{part}/3$ [9]) and other kinetic parameters that determine the rates of supply of target species towards the nanopores openings, its diffusion inside the nanopores and finally the rate of its adsorption/desorption at the walls. It should be noted that an efficient system (mixture of mesoporous particles) ought to contain a sufficient number of active sites in order to achieve a high level of sequestration and the kinetics of the process depends on the relative amounts of target species and active sites. The time efficiency of the system is best analyzed by considering characteristic times when f reaches an indicative value chosen here to be 0.75, which corresponds to the moment when the mesoporous material has extracted the amount of target species corresponding to 75% of its capacity.

II. THEORY

In this section, for the sake of convenience, we repeat the dimensionless formulation of the mass transport and adsorption problem [9] corresponding to significantly large nanopores with diameters of at least several molecular sizes (2D formulation) which permits classical diffusion of target species inside such nanopores. Fig. 1 shows the schematic representation of a single spherical particle immersed into a solution of target species under hydrodynamic mixing conditions exposing one nanotube within the particle core lined with active adsorption sites. Each particle is thus surrounded by a stagnant hydrodynamic diffusion layer which may be defined as a superposition of diffusion layers created due to diffusion of target species into each nanopore opening. Once inside the nanopore, target species travels by classical diffusion if the nanopore is sufficiently wide and/or by site-hopping diffusion along nanopore walls. Fig. 1 shows the normalized coordinate system inside a single nanopore.

In this work we focus on the 2D model of diffusion inside the nanopores which implies that the latter must be at least several target molecular sizes in diameter. The following mathematical equations describe the diffusion of target species occurring in the nanopore core solution with the same diffusion rate as in the bulk solution, which is coupled with adsorption at nanopore walls and diffusion by hopping between the active sites at the wall surface with the relative diffusion rate $\eta_{sh} = D_{site\ hopping} / D_{bulk}$ and the variations of the bulk solution concentration [9]:

$$\frac{\partial a}{\partial \tau} = \frac{\partial^2 a}{\partial y^2} + \varepsilon\left(\frac{\partial^2 a}{\partial \chi^2} + \frac{1}{\chi}\frac{\partial a}{\partial \chi}\right); \qquad (1)$$

$$\frac{\partial \theta}{\partial \tau} = \eta_{sh}\frac{\partial^2 \theta}{\partial y^2} + \lambda_0\left[(1-\theta)a - \theta\kappa\right]; \qquad (2)$$

$$\frac{dc}{d\tau} = -\upsilon\varphi(c - < a >_{y=0}) = -\upsilon\varphi\left(c - 2\int_0^1 a_{y=0}\chi d\chi\right), \qquad (3)$$

where $y = x/L$ and $\chi = \rho/R_{pore}$ are the normalized nanopore axial and radial coordinates, respectively, and $\varepsilon = (L/R_{pore})^2$.

The system (1)-(3) is associated with the following initial conditions ($\tau = 0$):

$$c = 1; \qquad (4a)$$

$$0 < y \le 1,\ 0 \le \chi \le 1:\ a(y,\chi,0) = 0,\quad \theta(y,0) = 0; \qquad (4b)$$

$$y = 0, \quad 0 \le \chi \le 1: \ a(0,\chi,0) = 1, \quad \theta(0,0) = 0, \tag{4c}$$

and boundary conditions ($\tau > 0$):

$$0 \le y < 1, \ \chi = 0: \ \left(\partial a/\partial\chi\right)_{\chi=0} = 0; \tag{5a}$$

$$y = 1, \ 0 \le \chi \le 1: \ \left(\partial a/\partial y\right)_{y=1} = 0; \tag{5b}$$

$$y = 1, \quad \chi = 1: \ \left(\partial\theta/\partial y\right)_{y=1} = 0; \tag{5c}$$

$$0 \le y < 1, \ \chi = 1: \ \left(\frac{\partial a}{\partial\chi}\right)_{\chi=1} = -\frac{\lambda_0\Xi_0}{2\varepsilon}\left[(1-\theta)a - \theta\kappa\right]; \tag{5d}$$

$$y = 0, \ 0 \le \chi \le 1: \ \left(\frac{\partial a}{\partial y}\right)_{y=0} = -\varphi(c - a_{y=0}); \tag{5e}$$

$$y = 0, \quad \chi = 1: \ \left(\partial\theta/\partial y\right)_{y=0} = 0. \tag{5f}$$

Equations (1)-(3) describe the evolution of the three main quantities that reflect the system behavior: normalized concentration of target species inside the nanopore $a = C/C_0^b$ (where C is the concentration, C_0^b is the initial bulk concentration of target species), normalized bulk concentration of target species $c = C^b/C_0^b$ and adsorption wall coverage, θ, representing the fraction of occupied active chemical sites inside the nanotube. Adsorption kinetics are defined by the dimensionless adsorption rate constant $\lambda_0 = k_{ads}L^2C_0^b/D_{bulk}$, where k_{ads} is the real adsorption rate constant (in $M^{-1}s^{-1}$), and the dimensionless pore storage parameter $\Xi_0 = (2\pi R_{pore}L)\Gamma_{site}/[(\pi R_{pore}^2L)C_0^b] = Q_{max}^{wall}/Q_{max}^{pore}$ representing the ratio of the target species amount storable by nanopore walls and that contained in the nanopore core volume at initial concentration, with Γ_{site} being the surface concentration of active sites.

We should remark here that the rate of decrease of the bulk concentration of target species due to the adsorption of the latter at the nanopore walls depends on (i) the mass transport conditions at the entrance to a single nanopore (including the concentration change across the pore entrance) and (ii) the effective number of all nanopores in the particle mixture. The concentrations in the bulk solution and that inside the pore are coupled through equations (3) and (5e). The effects of converging diffusion from the outer boundary of the hydrodynamic diffusion layer formed around a particle towards a single nanopore opening are taken into account by the parameter $\varphi = (L/\delta)(1+\delta/R_{part})(1+\omega/R_{pore})^2$ which describes the ensuing amplification of the target species flux, with R_{part} being the nanoporous particle radius. On the other hand, the parameter $\upsilon = \frac{4\pi R_{part}^3N_{part}}{3V^b}\left(\frac{R_{pore}}{R_{pore}+\omega}\right)^2$, where N_{part} is the total number of nanoporous particles in the assembly and V^b bulk solution volume, gives the ratio between the total volume of the pores and the bulk solution volume, thus characterizing the particle mixture as a whole (see below).

It should be noted that differential equation (3) introduces a slight simplification of the real physical picture of diffusion at the nanopore entrance through considering the average concentration over the nanopore entrance, $< a >_{y=0}$. However, this simplification has a minor effect on the overall model since any variations of the target species concentration along the nanopore radius occurring due to converging diffusion into the nanopore are smoothed out as soon as the diffusion front penetrated into the nanopore by more than a few its radii. Since in real systems the nanopore length greatly exceeds its radius, differential equation (3) is accurate for the whole duration of interest of the diffusion-adsorption process except the very beginning of it (which is too short to be perceived experimentally).

The effect of site-hopping diffusion (described by the first term on the right-hand side of (2)) onto the overall kinetics of target species sequestration is expected to be extremely minute due to redistribution of adsorbed target ions through to their exchanges between active sites being significantly slower than diffusion in the bulk solution.

III. Analysis of the Models and General Theoretical Results

A. Adsorption effectiveness

It is clear that high efficiency of inorganic particles-"sponges" aimed at selective sequestration of desired ions may be achieved under the conditions when adsorption of the target species is very strong compared to its desorption. Therefore in the following analysis we assume that $K_{des} = k_{des}/k_{ads}$, the desorption equilibrium constant introduced in [9], where k_{des} is the desorption rate constant in s^{-1}, is negligibly small so that the dimensionless parameter $\kappa = K_{des}/C_0^b$ may also be assumed to have so negligible a value that it does not affect the system behavior. Note that this simplification corresponds to an experimentally desired situation and depends only on the reactivity of the active sites.

Next we wish to establish the conditions corresponding to high adsorbing capacity of mesoporous organosilica particle mixtures of N_{part} particles with respect to a given solution volume V^b containing the target species at the initial concentration C_0^b. It was established in [9] that the normalized limiting concentration at $\tau \to \infty$ of target species in the bulk solution is given by the following expression:

$$c_\infty = \frac{1-\kappa(1+\upsilon)-\upsilon\Xi_0+\sqrt{(1-\kappa(1+\upsilon)-\upsilon\Xi_0)^2+4\kappa(1+\upsilon)}}{2(1+\upsilon)}, \tag{6}$$

which takes into account the limiting adsorptive wall coverage that depends on adsorption-desorption kinetics. Under the assumption of negligible desorption rate (viz., $\kappa \to 0$) the

normalized limiting concentration of target species simplifies into:

$$c_\infty = \frac{1-\upsilon\Xi_0 + \left|1-\upsilon\Xi_0\right|}{2(1+\upsilon)}. \quad (7)$$

The limiting concentration depends exclusively on two dimensionless parameters: υ and Ξ_0. The first parameter, υ, reflects the ratio of the cumulative volume of all pores in all particles and the solution volume:

$$\upsilon = \frac{4\pi R_{part}^3 N_{part}}{3V^b}\left(\frac{R_{pore}}{R_{pore}+\omega}\right)^2 = \frac{V_{pore}^{tot}}{V^b}. \quad (8)$$

The second parameter, Ξ_0, indicates the potential efficiency of adsorptive removal of target species from the solution and is equal to the ratio between the maximum adsorption capacity of the pore walls and the quantity of target species initially present in the pore bulk solution at its initial concentration C_0^b (see above).

It is clear that highest efficiency of the system is achieved when c_∞ is sufficiently close to zero, i.e. when most of the target species may be extracted from the solution by mesoporous particles. Thus, it is directly apparent from (7) that the limiting concentration c_∞ is identical zero when

$$\upsilon \geq \Xi_0^{-1}, \quad (9)$$

which corresponds to complete depletion of the solution. On the other hand, this result reflects the fact that complete extraction of the target species from the solution is possible only when the number of active sites in all the particles present in the solution exceeds the number of target molecules or ions in the initial solution, since

$$\upsilon\Xi_0 = \frac{N_{part}\left(\frac{4\pi R_{part}^2}{\pi(R_{pore}+\omega)^2}\right)(2\pi R_{pore}L)\Gamma_{site}}{C_0^b V^b} = \frac{Q_{max}^{wall\ tot}}{Q_0^b}, \quad (10)$$

which should be not less than unity for an efficient system.

It should be noted that, from the point of view of efficiency, one also should impose an upper limit on the parameter υ in order to define the maximum ratio of the particles volume to that of the solution.

B. Kinetics of target species sequestration

Equation (7) represents an important result concerning the *potential* (thermodynamic) efficiency of the system, however, the kinetics of the overall process is crucial for the time required to reach the desired level of target species sequestration (and hence the *practical* efficiency) depends on the reactivity of the active sites lining the nanopore walls, their diffusional accessibility as well as the rate of supply of target species to the nanopore entrances and the rate of the bulk concentration decay. This is an important factor since under effective regimes of application the particles are confined inside a reactor traversed by the fluid containing the target ion to be removed by the particles. Therefore, what matters is the time duration required for a nanopore to fill up to a given fraction of its nominal capacity, which should be comparable with reasonable residence time of the fluid to beremediated in the reactor. Hence, in the following we present data for the dimensionless times $\tau_{75\%}$ necessary to reach 75% of the thermodynamic capacity reflected by (7), i.e. times corresponding to the moments when the quantity $f(\tau) = (1-c(\tau))/(1-c_\infty)$ reaches 0.75. In all the calculations quoted hereafter the value of the dimensionless desorption equilibrium constant κ was kept at 10^{-6} to ensure that desorption effects are indeed negligible.

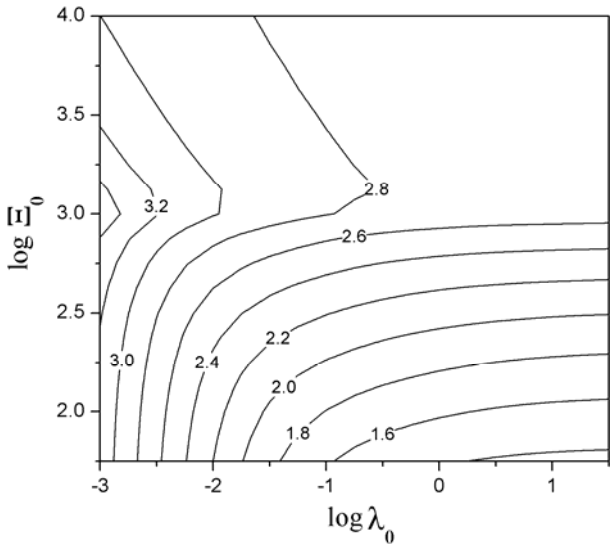

Fig. 3. Dependence of $\log\tau_{75\%}$ on λ_0 and Ξ_0.

It is clear that the dimensionless mathematical model given by (1)-(5) depends on five independent dimensionless parameters being λ_0, Ξ_0, ε, φ and υ (see [9] and above for the definitions). First we investigate how the interplay between the adsorption kinetics (λ_0) and relative quantity of adsorption sites (Ξ_0) determines the dimensionless time required to reach the acceptable level of solution sequestration (75% in our case). It is evident from Fig. 3 that the distribution of $\tau_{75\%}$ mostly depends on the parameter Ξ_0 and the dependence on the kinetic parameter λ_0 reveals itself only for sufficiently low values of λ_0 as predicted in [9] (see the schematic kinetic zone diagram in Fig. 2 and Fig. 4b of ref. [9]). When the adsorption rate λ_0 is extremely fast the process becomes diffusion-limited, in which case the apparent pore filling rate depends on the parameter Ξ_0 which results in the sole dependence on this parameter at high λ_0. When the adsorption kinetics are slow compared to diffusion, the diffusion-adsorption behavior inside the nanopores is more complex and is dictated by Ξ_0. In the case of low Ξ_0 the overall rate of adsorption is low so that nanotubes are filled before any effective reaction may start which results in virtually uniform growth of adsorption coverage in the whole nanopore. However, when there is a large excess of adsorption

sites the propagation of target species into the pore slows down (similarly to the fast adsorption kinetics limit) but in this case due to a large adsorptive capacity of the walls which leads to almost identical temporal development of the concentration and coverage profiles.

The distribution of the quantity $\tau_{75\%}$ presented in Fig. 3 must be considered together with the limiting solution sequestration, which is given by (7), as a function of $\log(\upsilon\Xi_0)$ (note that the value $\log\Xi_0 = 3$ approximately corresponds to $\log(\upsilon\Xi_0) = 0$ which corresponds to the conditions required for the number of active sites to equal the number of target species molecules or ions). As evident from Fig. 3, the time $\tau_{75\%}$ first increases and then either decreases with increasing Ξ_0 for low values of λ_0 or reaches a plateau for larger values of λ_0. This occurs due to the following reasons. When Ξ_0 is small the quantity of the target species that may be taken from the solution by the particles is also small which implies that the sequestration level of 75% is quickly reached. When Ξ_0 increases, the number of available sites also increases and more of target species has to be i) delivered to the active sites and ii) bound by them. This leads to the increase of $\tau_{75\%}$. However, further increase of Ξ_0 corresponds to a situation when the capacity of the pore walls becomes larger than the amount of target species in the solution (i.e. when $\upsilon\Xi_0 > 1$) and the number of active sites is no longer a limiting factor in sequestration efficiency. Thus for low values of λ_0 the dimensionless time $\tau_{75\%}$ decreases due to the increasing abundance of active sites while for large values of λ_0 this quantity reaches a plateau due to immediate binding of all target species entering the nanopores. Under the latter conditions the value of $\tau_{75\%}$ is limited exclusively by the rate of transport of target species towards nanopore openings (see below). It is also worth to note that for practical applications one wishes to reach a high level of sequestration of the target species which corresponds to the conditions when $\upsilon\Xi_0 \geq 1$ (see above), i.e. when all target species ions or molecules may be extracted from the solution at time infinity ($c_\infty = 0$) as follows from (7). Therefore only the corresponding parts of the plots in Fig. 3 are of practical interest.

Let us now investigate the dependence of $\tau_{75\%}$ on the parameters ε and φ which define the geometry of the system and the rate of supply of target species to the mesopore entrance. The ranges of these parameters are limited due to the physical meanings of real parameters composing these dimensionless quantities. Thus we shall not consider values of ε smaller than 100 which corresponds to the case when the average pore length is only 10 times its radius. For larger pore radii the model may introduce a significant bias due to the original geometrical assumptions. The value of $\varphi = (L/\delta)(1+\delta/R_{part})(1+\omega/R_{pore})^2$ is also limited from below due to the fact that $(1+\omega/R_{pore})^2 \approx 1$ and $(L/\delta)(1+\delta/R_{part}) = (R_{part}/\delta+1)/3$. Hence the lower bound for φ is $1/3$ (which corresponds to infinitely thin nanopore walls and still bulk solution giving rise to infinite diffusion layer).

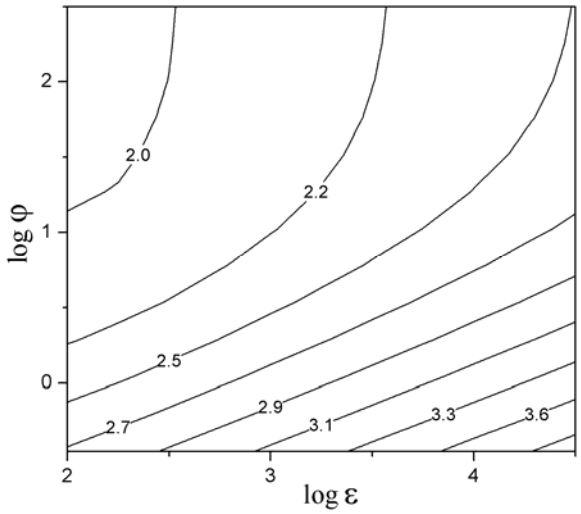

Fig. 4. $\log\tau_{75\%}$ as a function of parameters ε and φ for constant product $\upsilon\Xi_0 = 1$ and $\lambda_0 = 0.1$.

The dependence of $\tau_{75\%}$ on ε and φ was simulated while keeping the product $\upsilon\Xi_0$ equal to unity so that the number of available adsorptive sites always equals the number of target species molecules or ions. In this case the resulting data reflect exclusively the effects of nanopore geometry (through the variation of ε which may be interpreted as variation of nanopore radius R_{pore}) and rate of supply of target species from the solution bulk to nanopore entrance (represented by φ which in turn depends on the nanotube packing parameter ω as well as on the thickness of diffusion layer δ as imposed by solution hydrodynamic mixing). However, in doing so one needs to ensure that the actual density of active sites at pore walls remains the same for all values of ε, which is achieved by fixing the value of the dimensionless quantity $\Gamma_{site}/(LC_0^b)$ and recalculating the values $\Xi_0 = 2\sqrt{\varepsilon}\times\Gamma_{site}/(LC_0^b)$ and $\upsilon = \Xi_0^{-1}$. Therefore changing ε leads to changing values of two other parameters. The simulation results obtained for the parameter values $\lambda_0 = 0.1$, $\Gamma_{site}/(LC_0^b) = 5.35$ are shown in Fig. 4.

As expected, the values of $\tau_{75\%}$ are lower for low values of ε (i.e., for larger pores since this facilitates diffusional supply) and for high values of φ which corresponds e.g. to thin diffusion layer around particles and hence to faster supply of target species to nanopore entrances. It is also evident from Fig. 4 that when the diffusion layer is sufficiently thin (large φ) the value of $\tau_{75\%}$ becomes virtually independent of φ

which indicates that in this case the pore geometry is the main limiting factor determining the time-efficiency of the system. On the other hand, when the value of φ is not very high (i.e. less than ca. 0.75) the rate of diffusion inside the nanopore appears much faster than the rate of supply of target species towards the nanopore entrance. Under these circumstances the time $\tau_{75\%}$ necessary to achieve 75% sequestration with respect to c_∞ is limited by the rates of target species supply and its adsorption at the pore walls, i.e. according to (5d) and (5e)

$$\tau_{75\%} \propto \frac{\lambda_0 \Xi_0 \varphi}{2\varepsilon}. \qquad (11)$$

Bearing in mind that $\Xi_0 = 2\sqrt{\varepsilon} \times \Gamma_{site} / (LC_0^b)$ one can devise that within the specified range of φ the time $\tau_{75\%}$ is constant whenever

$$\log\varphi - \frac{\log\varepsilon}{2} = \text{const}. \qquad (12)$$

This relationship is clearly observable in the lower part of Fig. 4 where the contour lines of $\tau_{75\%}$ are virtually straight and have the slope of 1/2.

IV. Computational details

The computer program for the presented numerical simulations was written in Borland Delphi 7 Professional Edition and executed on a PC equipped with Pentium D processor at 2.8 GHz and 512 MB of RAM.

The model was discretized using the fully implicit finite difference scheme [10] on a uniform grid in both spatial directions and time. The typical grid size was $Ny \times N\chi \times N\tau = 100 \times 20 \times 2000$ which ensured numerical convergence of better than 1% for all considered parameter ranges.

V. Conclusion

Numerical simulation has allowed the solution of the system of partial and ordinary differential equations comprising the mathematical model of selective sequestration of target species by spherical mesoporous organosilica particles. Thorough theoretical analysis and simulation of the case of sufficiently large nanopores (with radii of at least several molecular sizes) has yielded the dependences of characteristic time $\tau_{75\%}$ necessary for reaching 75% sequestration on governing kinetic parameters. These results may be employed for the optimization of mesoporous materials for designing highly efficient systems to be applied for filtration or sequestration of desired ions or molecules from dilute solutions.

Acknowledgment

The author wishes to express his gratitude to Professor Christian Amatore (ENS, Paris, France) and Dr Alain Walcarius (Nancy University, Nancy, France) for their help in conducting this research.

References

[1] H. Yang, G.A. Ozin, C.T. Kresge, "The role of defects in the formation of mesoporous silica fibers, films, and curved shapes," *Adv. Mater*., vol. 10, pp. 883-887, Aug. 1998.

[2] I. Oda, K. Hirata, S. Watanabe, Y. Shibata, T. Kajino, Y. Fukushima, S. Iwai, S. Itoh, "Function of membrane protein in silica nanopores: incorporation of photosynthetic light-harvesting protein LH2 into FSM," *J. Phys. Chem. B*, vol. 110, pp. 1114-1120, Jan. 2006.

[3] P.V. Braun in *Nanocomposite Science and Technology*, P.M. Ajayan, L.S. Schadler, P.V. Braun, Eds. Wenheim: Wiley-VCH Verlag GmbH & Co. KGaA, 2003, pp. 155-214.

[4] A. Walcarius, E. Sibottier, M. Etienne, J. Ghanbaja, "Electrochemically assisted self-assembly of mesoporous silica thin films," *Nature Materials*, vol. 6, pp. 602-608, Aug. 2007.

[5] M. Etienne, A. Quach, D. Grosso, L. Nicole, C. Sanchez, A. Walcarius, "Molecular transport into mesostructured silica thin films: electrochemical monitoring and comparison between *p*6*m*, *P*6$_3$/*mmc*, and *Pm*3*n* structures," *Chem. Mater*., vol. 19, pp. 844-856, Feb. 2007.

[6] H. Han, H. Frei, "Visible light absorption of binuclear $TiOCo^{II}$ charge-transfer unit assembled in mesoporous silica," *Microporous and Mesoporous Materials*, vol. 103, pp. 265-272, Jun. 2007.

[7] G. Wang, B. Zhang, J.R. Wayment, J.M. Harris, H.S. White, "Electrostatic-gated transport in chemically modified glass nanopore electrodes," *J. Am. Chem. Soc*., vol. 128, pp. 7679-7686, Jun. 2006.

[8] S. Brandès, G. David, C. Suspène, R. J. P. Corriu, R. Guilard, "Exceptional affinity of nanostructured organic-inorganic hybrid materials towards dioxygen: Confinement effect of copper complexes," *Chem. Eur. J*., vol. 13, pp. 3480-3490, Apr. 2007.

[9] C. Amatore, "Theoretical trends of diffusion-reaction into tubular nano- and mesoporous structures: A general physicochemical and physicomathematical modeling," *Chem. Eur. J*., to be published.

[10] R.D. Richtmyer, K.W. Morton, *Difference methods for initial-value problems*, 2-nd ed. New York: Wiley-Interscience, 1967.

Oleksiy V. Klymenko is a Senior Scientist of the Mathematical and Computer Modelling Laboratory of Kharkov National University of Radioelectronics (KNURE). He received the D. Phil. degree in computational electrochemistry from the University of Oxford, UK in 2004. In 2006 he received the Candidate of Physical and Mathematical Sciences (equivalent to PhD) from the A.N. Podgorny Institute for Mechanical Engineering Problems of the National academy of Sciences of Ukraine, Kharkov, Ukraine. His research interests include mathematical physics, mathematical modelling in physical chemistry and biology, numerical methods, solution of inverse problems in sciences.